Available online at www.sciencedirect.com
ScienceDirect
Journal of Power Sources 161 (2006) 1346–1355
JOURNAL OF POWER SOURCES
www.elsevier.com/locate/jpowsour

Online estimation of the state of charge of a lithium ion cell

Shriram Santhanagopalan, Ralph E. White *

Center for Electrochemical Engineering, Department of Chemical Engineering, University of South Carolina, Columbia, SC 29208, United States

Received 14 March 2006; received in revised form 27 April 2006; accepted 28 April 2006
Available online 19 June 2006

Abstract

A procedure to predict the state of charge of a lithium ion cell using experimental data (cell potential versus time), as it becomes available, is presented. The procedure is based on the physics of the system and provides a realistic estimate of the state of charge of the cell as a function of time, for a given set of properties of the electrodes. An electrochemical cell model is used to obtain an extended Kalman filter (EKF) for estimating the state of charge (SOC) of a lithium ion cell in which the negative electrode is the limiting electrode. The method could also be used for a cell in which the positive electrode is limiting.
© 2006 Elsevier B.V. All rights reserved.

Keywords: State of charge; Lithium ion battery; Online; Extended Kalman filter; Parameter estimation

1. Introduction

The phrase state of charge (SOC) is routinely used to describe the performance of a lithium ion cell [1]. Numerous approaches have been presented in refs. [2–28] to monitor the SOC of a cell; most of these are for lead-acid batteries. These include, but are not limited to, following a physical property like the internal resistance of the cell or the electrolyte density [3,4], measurement of the cell impedance [5–8], optical methods [9], eddy current methods [10], equivalent circuit analysis of the charge/discharge and/or impedance curves [11–18,22], techniques employing a Kalman filter [19–21], techniques based on fuzzy logic [23–25] and coulomb-counting [26,27]. The model by Tenno et al. for the VRLA battery [2] is valid only under overcharge. Piller et al. [28] provide a good overview of most of these methods. Huet [5] provides an extensive review of impedance measurements for determination of the SOC for lead-acid and nickel–cadmium cells. Verbrugge et al. [14–17] discuss the utility of circuit analog models in the recursive estimation of parameters to predict battery performance in the context of electric vehicles. Fuzzy-logic based models that can be readily implemented in hardware are discussed in the work by Salkind et al. [23]. Hansen and Wang [12] present a pattern recognition algorithm that reduces the computational effort for circuit-based models developed using ADVISOR [13] and makes them suitable for real-time embedded system applications. Nanjudaiah and Koch [26] developed a cycle-life sensor for a Li/Li^+ half cell by inserting a Pt microelectrode inside the cell. Martinet et al. [18] present a correlation between the electrochemical noise in a battery system and its state of charge.

In methods employing circuit analogy, the parameter that is tracked to estimate the state of charge is most often empirical with little physical significance. The coulomb-counting procedure is not reliable since not all the current supplied goes to charging the cell and the charge lost to any undesired side reaction [30] is not included. Similarly, the fuzzy logic based methods rely on the training data supplied. Hence the results from these models are of limited value in predicting the SOC or SOH of a battery. Consequently, there arises a need for state of charge estimation based on the physics of the cell. Unfortunately, the computational time required to solve rigorous battery models [29] repeatedly practically eliminates the utility of physics-based models that are used to characterize the SOC of the cell. Intermediate models (i.e., extension of circuit analog models) were presented by Plett [19–21], but these are too empirical to provide any insight into the system. Some of our recent publications [31–33] present a simple, computationally efficient, ordinary differential equation (ODE) model of the cell using the FORTRAN subroutine DDASL [34], that is capable of predicting well, the charge/discharge curves of a lithium ion cell, up to

* Corresponding author. Tel.: +1 803 777 3270; fax: +1 803 777 0973.
E-mail address: white@engr.sc.edu (R.E. White).

0378-7753/$ – see front matter © 2006 Elsevier B.V. All rights reserved.
doi:10.1016/j.jpowsour.2006.04.146

Nomenclature

a_j	specific surface area of the electrode 'j' ($m^2\ m^{-3}$)
$c_{1,j}$	concentration of lithium in the solid phase ($mol\ m^{-3}$)
c_0	concentration of the electrolyte ($mol\ m^{-3}$)
$c_{1,j}^{avg}$	average concentration of lithium in the solid phase ($mol\ m^{-3}$)
$c_{1,j}^{max}$	maximum concentration of lithium in the solid phase ($mol\ m^{-3}$)
$c_{1,j}^{s}$	concentration of lithium at the surface of the sphere ($mol\ m^{-3}$)
$c_{1,j}^{0}$	initial concentration of lithium in the solid phase ($mol\ m^{-3}$)
$D_{1,j}$	diffusion coefficient of lithium in the solid phase inside electrode 'j' ($m^2\ s^{-1}$)
$\boldsymbol{e}$	weighted sum-squared error
$\boldsymbol{f}$	forcing function matrix
F	Faraday's constant (96,487 C/equivalent)
$\boldsymbol{F}$	linearized forcing function matrix
$\boldsymbol{G}(t)$	matrix of process noise coefficients
$\boldsymbol{h}$	function of the estimated states
$\boldsymbol{H}$	linearized system matrix
$\boldsymbol{J}_j$	flux entering electrode j (A)
k_j	rate constant for the electrochemical reaction at the surface ($m^{2.5}\ mol^{-0.5}\ s^{-1}$)
$\boldsymbol{K}$	filter gain
n	number of electrons transferred (=1)
$\boldsymbol{P}$	covariance matrix
Q	Variance of the process noise
r	radial coordinate (m)
R_j	radius of the particle in phase 'j' ($j=n, p$) (m)
R_{k+1}	variance of the measurement noise
t	time (s)
$\boldsymbol{u}(t)$	input function
U_j^{θ}	open circuit potential at the electrode 'j'.
$\underline{x}$	vector of the state variables
V_{cell}	cell potential (V)
$\boldsymbol{W}$	weight matrix
$\boldsymbol{y}$	vector of the predicted values of the output variables
$\mathbf{y}^*$	vector of the experimental values of the output variables
$\phi_{1,j}$	solid phase potential at the electrode 'j' (V)
θ_j	utility coefficient of electrode 'j'
θ_n	state of charge based on the negative electrode

and including the 1 C rate. In this work, our model is used to design an extended Kalman filter (EKF) to predict the state of charge of a lithium ion cell as it is charged or discharged. The model is regressed with synthetic data (cell potential as a function of time) to provide estimates of the solid phase concentrations as functions of time and hence, the state of charge of the cell can be monitored online. State of health (SOH) on the other hand provides information on aging of the cell. Cycling performance of the cell is not considered in this paper and hence SOH calculations are of little relevance in this context [20]. However, it must be mentioned that an extension of the present technique (currently being pursued in our laboratory) to study cycling behavior will yield the SOC as well as the SOH of the cell.

2. The Kalman filter

The term "filter" refers to a weighted least squares algorithm that can be used to minimize the effects of measurement noise [45]. A brief review of linear filters is provided in this section, followed by a direct analogy for the nonlinear case, which is of interest in the context of an electrochemical cell.

Let us say we have an approximate model of a system:

$$\begin{aligned} y_1(t) &= a_1 x_1(t) + b_1 x_2(t) \\ y_2(t) &= a_2 x_1(t) + b_2 x_2(t) \end{aligned} \tag{1}$$

where y_1 and y_2 are equivalents (in the model) of the variables that can be directly measured in an experiment, x_1 and x_2 are the state variables (in the model) to be estimated as a function of time, for given values of the constants a_i and b_i. The objective is to estimate and update the values of x_1 and x_2 as we progress in time.

The equation above can be written in the state-space form [45] as follows:

$$\boldsymbol{y} = \boldsymbol{H} \cdot \boldsymbol{x} \tag{2}$$

where the output vector is:

$$\boldsymbol{y} = \begin{bmatrix} y_1 \\ y_2 \end{bmatrix} \tag{3}$$

and the vector of states is:

$$\boldsymbol{x} = \begin{bmatrix} x_1 \\ x_2 \end{bmatrix} \tag{4}$$

$\boldsymbol{H}$ is the system matrix (or the matrix of coefficients):

$$\boldsymbol{H} = \begin{bmatrix} a_1 & b_1 \\ a_2 & b_2 \end{bmatrix} \tag{5}$$

Let y_1^* and y_2^* be the experimental values corresponding to the model predictions y_1 and y_2, respectively. From an experiment, we are able to measure y_1^* and y_2^* at various time steps, for example, t_k and t_{k+1}. Let us denote these values as $y_{1,k}^*$ and $y_{2,k}^*$ at $t=t_k$, and $y_{1,k+1}^*$ and $y_{2,k+1}^*$ at $t=t_{k+1}$. The corresponding values in the model are $y_{1,k}$ and $y_{2,k}$ for $t=t_k$ and $y_{1,k+1}$ and $y_{2,k+1}$ for $t=t_{k+1}$.

In a set of experimental data, all the data points need not be equally weighted—some allowance must be provided to account for the deviations due to experimental error. Let the weight associated with a data point at time $t=t_k$ be $W_{i,k}$ (i.e., the weight for

$y^*_{1,k}$ at $t = t_k$ will be $W_{1,k}$). Then the weighted sum-squared residual is given by:

$$\boldsymbol{e}_k = \tfrac{1}{2}[(\underline{y}_k - \underline{y}^*_k)^T \boldsymbol{W}_k (\underline{y}_k - \underline{y}^*_k)] \tag{6}$$

where

$$\boldsymbol{W}_k = \begin{bmatrix} W_{1,k} & 0 \\ 0 & W_{2,k} \end{bmatrix} \tag{7}$$

assuming that there is no correlation between the errors. Note that if 'j' is the number of state variables, then the residual is given by:

$$\boldsymbol{e}_k = \tfrac{1}{2}\sum_j W_{j,k}(y_{j,k} - y^*_{j,k})^2 \tag{8}$$

Our objective then, is to estimate the state variables ($x_{1,k}$ and $x_{2,k}$) such that the error between the predictions made ($y_{1,k}$ and $y_{2,k}$) using the estimates and the experimental measurements is minimal: i.e., minimize the expression for the sum squared error given by Eq. (8), with respect to the state variables. To achieve this, we find the first derivatives of the function to be minimized ($\boldsymbol{e}_k$) with respect to each of the state variables ($x_{1,k}$ and $x_{2,k}$) and set them equal to zero:

$$\nabla_{\boldsymbol{x}_k} \boldsymbol{e}_k = \frac{1}{2}\sum_{j=1}^{n} 2\frac{\partial y_{j,k}}{\partial x_{j,k}} W_{j,k}(y_{j,k} - y^*_{j,k}) = \boldsymbol{0} \quad \text{for } n = 1, 2 \tag{9}$$

Rewriting Eq. (9) in the state-space form, we have:

$$\nabla_{\boldsymbol{x}_k} \boldsymbol{e}_k = \boldsymbol{H}_k^{\mathrm{T}} \boldsymbol{W}_k (\boldsymbol{y}_k - \boldsymbol{y}^*_k) = 0 \tag{10}$$

Since $\boldsymbol{y}_k = \boldsymbol{H}_k \times \boldsymbol{x}_k$ Eq. (10) can be rewritten as follows:

$$\nabla_{\boldsymbol{x}_k} \boldsymbol{e}_k = \boldsymbol{H}_k^{\mathrm{T}} \boldsymbol{W}_k (\boldsymbol{H}_k \cdot \boldsymbol{x}_k - \boldsymbol{y}^*_k) = 0 \tag{11}$$

Eq. (11) yields:

$$\boldsymbol{x}_k = (\boldsymbol{H}_k^{\mathrm{T}} \boldsymbol{W}_k \boldsymbol{H}_k)^{-1} \boldsymbol{H}_k^{\mathrm{T}} \boldsymbol{W}_k \boldsymbol{y}^*_k \tag{12}$$

We now have $\boldsymbol{x}_k$ in terms of $\boldsymbol{y}^*_k$. The next step is to find $\boldsymbol{x}_{k+1}$ in terms of $\boldsymbol{x}_k$ and $\boldsymbol{y}^*_{k+1}$. At time t_{k+1} we have data points from t_k and t_{k+1}. Hence using similar arguments [45] used to derive (12) we have:

$$\begin{aligned} \boldsymbol{x}_{k+1} = {} & (\boldsymbol{H}_k^{\mathrm{T}} \boldsymbol{W}_k \boldsymbol{H}_k + \boldsymbol{H}_{k+1}^{\mathrm{T}} \boldsymbol{W}_{k+1} \boldsymbol{H}_{k+1})^{-1} \\ & \times (\boldsymbol{H}_k^{\mathrm{T}} \boldsymbol{W}_k \boldsymbol{y}^*_k + \boldsymbol{H}_{k+1}^{\mathrm{T}} \boldsymbol{W}_{k+1} \boldsymbol{y}^*_{k+1}) \end{aligned} \tag{13}$$

Substituting (13) into (12) and simplifying we obtain:

$$\begin{aligned} \boldsymbol{x}_{k+1} = {} & \boldsymbol{x}_k + (\boldsymbol{H}_k^{\mathrm{T}} \boldsymbol{W}_k \boldsymbol{H}_k + \boldsymbol{H}_{k+1}^{\mathrm{T}} \boldsymbol{W}_{k+1} \boldsymbol{H}_{k+1})^{-1} \\ & \times \boldsymbol{H}_{k+1}^{\mathrm{T}} \boldsymbol{W}_{k+1} (\boldsymbol{y}^*_{k+1} - \boldsymbol{H}_{k+1} \boldsymbol{x}_k) \end{aligned} \tag{14}$$

Eq. (14) is of the form:

$$\boldsymbol{x}_{k+1} = \boldsymbol{x}_k + \boldsymbol{K}_{k+1}(\boldsymbol{y}^*_{k+1} - \boldsymbol{H}_{k+1} \boldsymbol{x}_k) \tag{15}$$

where

$$\boldsymbol{K}_{k+1} = (\boldsymbol{H}_k^{\mathrm{T}} \boldsymbol{W}_k \boldsymbol{H}_k + \boldsymbol{H}_{k+1}^{\mathrm{T}} \boldsymbol{W}_{k+1} \boldsymbol{H}_{k+1})^{-1} \boldsymbol{H}_{k+1}^{\mathrm{T}} \boldsymbol{W}_{k+1} \tag{16}$$

is the filter gain and

$$\boldsymbol{P}_{k+1} = (\boldsymbol{H}_k^{\mathrm{T}} \boldsymbol{W}_k \boldsymbol{H}_k + \boldsymbol{H}_{k+1}^{\mathrm{T}} \boldsymbol{W}_{k+1} \boldsymbol{H}_{k+1})^{-1} \tag{17}$$

is the covariance matrix.

3. Extension to the nonlinear case

For the nonlinear case, the model equations are typically of the form:

$$\dot{\boldsymbol{x}}(t) = \boldsymbol{f}(\boldsymbol{x}(t), \boldsymbol{u}(t), t) + \boldsymbol{G}(t)\boldsymbol{W}(t) \tag{18}$$

$$\boldsymbol{y}(t) = \boldsymbol{h}(\boldsymbol{x}(t)) \tag{19}$$

where $\boldsymbol{W}(t)$ is the weight on the process noise $\boldsymbol{G}(t)$ and $\boldsymbol{u}(t)$ *is* the input. The experimental data is represented by:

$$\boldsymbol{y}^*_k = \boldsymbol{h}(\hat{\boldsymbol{x}}_k) + \boldsymbol{v}_k \tag{20}$$

where $\boldsymbol{v}_k$ is zero mean Gaussian noise associated with the measurements, whose variance is σ. The symbol $\hat{\boldsymbol{x}}_k$ is used to approximate the actual values of the discretized state variables $\boldsymbol{x}_k$. This approximation is essential because the nonlinear system does not have an exact solution like the linear case. The objective then, is to design a filter quite similar to Eq. (14) that can predict $\hat{\boldsymbol{x}}_{k+1}$ given $\hat{\boldsymbol{x}}_k$. This equation is of the form:

$$\hat{\boldsymbol{x}}_{k+1} = \hat{\boldsymbol{x}}_k + [\boldsymbol{K}(\hat{\boldsymbol{x}}_k)]_{k+1}(\boldsymbol{y}^*_k - \boldsymbol{h}(\hat{\boldsymbol{x}}_k)) \tag{21}$$

The main difference between Eqs. (21) and (15) is that the gain matrix ($\boldsymbol{K}(\hat{\boldsymbol{x}}_k)$) for the nonlinear case is a function of the state variables ($\hat{\boldsymbol{x}}_k$) and hence an iterative solution procedure is essential. Upon linearizing the model equations (Eqs. (18) and (19)) an equation set for an extended Kalman filter can be obtained. The linearized form of the matrices $\boldsymbol{f}$ and $\boldsymbol{h}$ are given by:

$$\boldsymbol{F} = \left.\frac{\partial(\boldsymbol{f}(\boldsymbol{x}(t), \boldsymbol{u}(t), t))}{\partial \boldsymbol{x}(t)}\right|_{\boldsymbol{x}(t)=\hat{\boldsymbol{x}}_k} \tag{22}$$

$$\boldsymbol{H}_k = \left(\frac{\partial(\boldsymbol{h}(\boldsymbol{x}(t)))}{\partial \boldsymbol{x}(t)}\right)_{\boldsymbol{x}(t)=\hat{\boldsymbol{x}}_k} \tag{23}$$

For known values of $\boldsymbol{G}(t)$ and σ the Riccati equation [41,45] can be used for the filter gain:

$$\boldsymbol{K}_{k+1} = \frac{Q \cdot \boldsymbol{P}_{k+1} \boldsymbol{H}_{k+1}^{\mathrm{T}}}{Q \cdot \boldsymbol{H}_{k+1} \boldsymbol{P}_{k+1} \boldsymbol{H}_{k+1}^{\mathrm{T}} + R_{k+1}} \tag{24}$$

$\boldsymbol{P}_{k+1}$ is the state error covariance defined by [45]:

$$\boldsymbol{P}_{k+1} = E\{\hat{\boldsymbol{x}}_{k+1}, \hat{\boldsymbol{x}}_{k+1}^{\mathrm{T}}\} \tag{25}$$

Q is the covariance of the process noise (i.e., $\boldsymbol{G}(t)\boldsymbol{W}(t)$). In this work, the weight matrix $\boldsymbol{W}$ is held constant over time, for simplicity and equals the identity matrix since the process noise is assumed to be uncorrelated. For this case, the covariance of the process noise is defined by [45]:

$$Q = E\{\boldsymbol{W}\boldsymbol{W}^{\mathrm{T}}\} \tag{26}$$

Table 1
List of parameters

Parameter	Unit	Anode	Cathode
Radius of the particle (R_j)	m	11×10^{-6}	12.5×10^{-6}
Rate constant (k_j)	$\text{mol}^{-(1/2)}\,\text{s}^{-1}$	4.907×10^{-5}	1.139×10^{-5}
Maximum lithium concentration ($c_{1,j}^{\max}$)	$\text{mol}\,\text{m}^{-3}$	51555	30555
Solid phase diffusion coefficient ($D_{1,j}$)	$\text{m}^2\,\text{s}^{-1}$	1.0×10^{-14}	3.9×10^{-14}
Mass of active material (m_j)	g	15.92	7.472
Electrolyte concentration (c_0)	$\text{mol}\,\text{m}^{-3}$		1000
Temperature (T)	K		298.15
Faraday's constant (F)	$\text{C}\,\text{mol}^{-1}$		96487.0
Gas constant (R)	$\text{J}\,\text{mol}^{-1}\,\text{K}^{-1}$		8.314

R_{k+1} is the covariance of the noise in the measurement (i.e., $\boldsymbol{v}_{k+1}$) given by [45]:

$$R_{k+1} = E\{\boldsymbol{v}_{k+1}\boldsymbol{v}_{k+1}^{\mathrm{T}}\} \tag{27}$$

The Riccati equation is a result of a transformation that seeks to replace a differential equation with an equivalent collection of uncoupled equations of lower order [43]. Two limiting cases are considered to illustrate the capabilities of Eq. (24): case (i) the measurement noise is much greater than the process noise (i.e., $R_{k+1} \gg Q$) and case (ii) the measurement noise is much less than the process noise (i.e., $R_{k+1} \ll Q$). For case (i), the Riccati equation (Eq. (24)) simplifies to:

$$\boldsymbol{K}_{k+1} = \frac{Q \cdot \boldsymbol{P}_{k+1}\boldsymbol{H}_{k+1}^{\mathrm{T}}}{Q \cdot \boldsymbol{H}_{k+1}\boldsymbol{P}_{k+1}\boldsymbol{H}_{k+1}^{\mathrm{T}} + R_{k+1}} \approx 0 \tag{28}$$

In other words, the gain matrix is not updated if the measurement noise is much greater than the process noise. For case (ii), Eq. (24) can be simplified to:

$$\boldsymbol{K}_{k+1} = \frac{Q \cdot \boldsymbol{P}_{k+1}\boldsymbol{H}_{k+1}^{\mathrm{T}}}{Q \cdot \boldsymbol{H}_{k+1}\boldsymbol{P}_{k+1}\boldsymbol{H}_{k+1}^{\mathrm{T}} + R_{k+1}} \approx (\boldsymbol{H}_{k+1})^{-1} \tag{29}$$

For this case, the gain matrix ($\boldsymbol{K}_{k+1}$) directly maps the noise ($\boldsymbol{v}_k$) in the output ($\boldsymbol{y}_k$) to the update in the state variable ($\hat{\boldsymbol{x}}_k$). Thus, the Riccati equation is capable of filtering the measurement noise out while retaining the process noise. The choice of Q and R_{k+1} are arbitrary—however, determination of an appropriate value for Q from the variance of experimental data is possible [42,46]. More details on these tuning parameters are provided below.

4. The single particle model

The single particle (SP) approach originally developed by Haran et al. [31] for the metal hydride battery and later extended to the lithium system [32,33] is used in this work. This model includes the assumption that each electrode of a lithium ion cell can be approximated by a single spherical particle whose surface area is scaled to that of the porous electrode. Further, concentration and potential changes in the solution phase are ignored. All parameters are held constant (see Table 1) and thermal effects are assumed to be negligible. No attempt is made in this work to model capacity fade [30] with cycling of the cell. Most of these assumptions can be readily relaxed [32] at the cost of a more sophisticated model. Fig. 1 provides a schematic of the SP model and the model equations are presented below.

Diffusion in the solid phase is governed by the Fick's laws [35] written in spherical coordinates:

$$\frac{\partial c_{1,j}}{\partial t} = D_{1,j}\frac{1}{r^2}\frac{\partial}{\partial r}\left(r^2\frac{\partial c_{1,j}}{\partial r}\right) \tag{30}$$

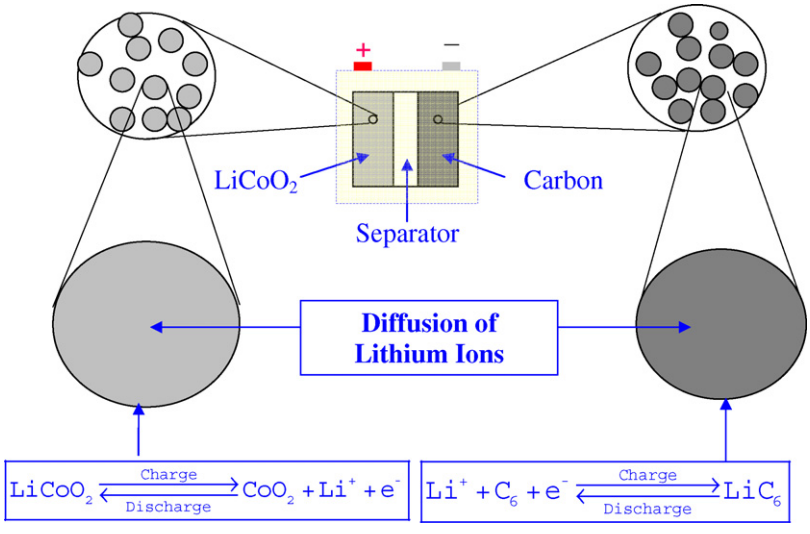

Fig. 1. A schematic representation of the single particle model.

$$c_{1,j}\big|_{t=0} = c^0_{1,j} \tag{31}$$

$$\left(\frac{\partial c_{1,j}}{\partial r}\right)_{r=0} = 0 \qquad \left(\frac{\partial c_{1,j}}{\partial r}\right)_{r=R_j} = -\frac{\boldsymbol{J}_j}{nFD_{1,j}a_j} \tag{32}$$

where $\boldsymbol{J}_j$ is the flux entering electrode 'j'. Eqs. (1)–(3) can be volume averaged [36,37] and the concentration inside the solid phase ($c_{1,j}$) can be expressed in terms of the concentration at the surface of the sphere ($c^s_{1,j}$) and the average concentration inside the sphere ($c^{\text{avg}}_{1,j}$). The resultant equations are:

$$\frac{\mathrm{d}c^{\text{avg}}_{1,j}}{\mathrm{d}t} + \frac{15D_{1,j}}{R_j}(c^{\text{avg}}_{1,j} - c^s_{1,j}) = 0 \tag{33}$$

$$c^{\text{avg}}_{1,j}\Big|_{t=0} = c^0_{1,j}$$

$$\boldsymbol{J}_j + \frac{5D_{1,j}}{R_j}(c^s_{1,j} - c^{\text{avg}}_{1,j})Fa_j = 0 \tag{34}$$

Butler-Volmer kinetics [38] is employed to represent the charge transfer reaction at the surface of the sphere:

$$\boldsymbol{J}_j = Fa_j k_j \sqrt{c^{\max}_{1,j} - c^s_{1,j}}\sqrt{c^s_{1,j}c_0}\left\{\exp\left(\frac{0.5F}{RT}[\phi_{1,j} - U^\theta_j]\right) - \exp\left(-\frac{0.5F}{RT}[\phi_{1,j} - U^\theta_j]\right)\right\} \tag{35}$$

Finally, since none of the above variables solved for ($\phi_{1,j}$, $c^s_{1,j}$, $c^{\text{avg}}_{1,j}$) are directly measurable from a functioning cell, the solid phase potentials of the individual electrodes are related to the cell voltage as follows:

$$V_{\text{cell}} = \phi_{1,p} - \phi_{1,n} \tag{36}$$

The open circuit potentials (U^θ_j) are empirical functions of the solid phase concentration ($c^s_{1,j}$ for the present case) obtained by fitting experimental data to polynomial expressions [40]. The expressions presented by Ramadass et al. [30] are used here:

$$U^\theta_n = 0.7222 + 0.1387\theta_n + 0.029\theta_n^{0.5} - \frac{0.0172}{\theta_n} + \frac{0.0019}{\theta_n^{1.5}} + 0.2808\mathrm{e}^{(0.90-15\theta_n)} - 0.7984\mathrm{e}^{(0.4465\theta_n - 0.4108)} \tag{37}$$

$$U^\theta_p = \frac{-4.656 + 88.669\theta_p^2 - 401.119\theta_p^4 + 342.909\theta_p^6 - 462.471\theta_p^8 + 433.434\theta_p^{10}}{-1.0 + 18.933\theta_p^2 - 79.532\theta_p^4 + 37.311\theta_p^6 - 73.083\theta_p^8 + 95.96\theta_p^{10}} \tag{38}$$

where

$$\theta_j = \frac{c^s_{1,j}}{c^{\max}_{1,j}} \tag{39}$$

is the utility coefficient. At the end of complete discharge, θ_j reaches a value of 1.0 for the positive electrode and 0.0 for the negative electrode in an ideal cell.

5. Online estimation of the state of charge

The SP model presented in the previous section needs further simplification to be rewritten in the form of Eqs. (18) and (19). Eqs. (33) and (34) can be combined and the resulting equation can be rewritten for each electrode in state space form as follows:

$$\begin{bmatrix} \dfrac{\mathrm{d}c^{\text{avg}}_{1,p}}{\mathrm{d}t} \\ \dfrac{\mathrm{d}c^{\text{avg}}_{1,n}}{\mathrm{d}t} \end{bmatrix} = \begin{bmatrix} -\dfrac{3}{R_p Fa_p}J_p \\ \dfrac{3}{R_n Fa_n}J_n \end{bmatrix} \tag{40}$$

For this case the equivalent of Eq. (19) is the expression for the cell potential (V_{cell}) obtained by combining Eqs. (35)–(39) to give:

$$V_{\text{cell}} = \phi_{1,p} - \phi_{1,n} = h(c^{\text{avg}}_{1,p}(t), c^{\text{avg}}_{1,n}(t), J_p, J_n) \tag{41}$$

V_{cell} corresponds to the output variable $y(t)$ since it is directly measurable. The vector $\boldsymbol{F}$ is linear for this model. As seen from Eq. (40), we have:

$$\boldsymbol{F} = \begin{bmatrix} -\dfrac{3}{R_p Fa_p}J_p \\ \dfrac{3}{R_n Fa_n}J_n \end{bmatrix} \tag{42}$$

The function h is nonlinear, and is dependent on the state variables ($c^{\text{avg}}_{1,p}(t)$ and $c^{\text{avg}}_{1,n}(t)$) and the input current. The experimental data for V_{cell} (represented by y^*_k in Eq. (20)) are simulated in this paper by adding a zero mean Gaussian noise ($\boldsymbol{v}_k$) with a variance of 0.1.

The state of charge of the cell (SOC) is represented by the ratio between the average concentration of lithium ($c^{\text{avg}}_{1,j}(t)$) inside the limiting electrode and the maximum concentration ($c^{\max}_{1,j}(t)$) inside that electrode. Most commercial lithium ion cells are limited by the performance of the negative electrode [44]. Hence, for illustrative purposes, the negative electrode is assumed to be the limiting electrode and the state of charge based on the negative electrode ($\theta_n(t)$) is given by:

$$\theta_n(t) = \frac{c^{\text{avg}}_{1,n}(t)}{c^{\max}_{1,n}(t)} \tag{43}$$

However, the technique is not limited to negative limited electrodes; an equivalent formulation can be done based on the average concentration of lithium inside the positive electrode, for the case of positive electrode limited cells.

6. Results and discussion

The process noise ($\boldsymbol{G}(t)\boldsymbol{W}$) is a measure of the inaccuracy of the model, while the measurement noise ($\boldsymbol{v}_k$) is a measure of external disturbance that corrupts the actual data collected from the system. Hence, the variance of the process noise (Q) and that

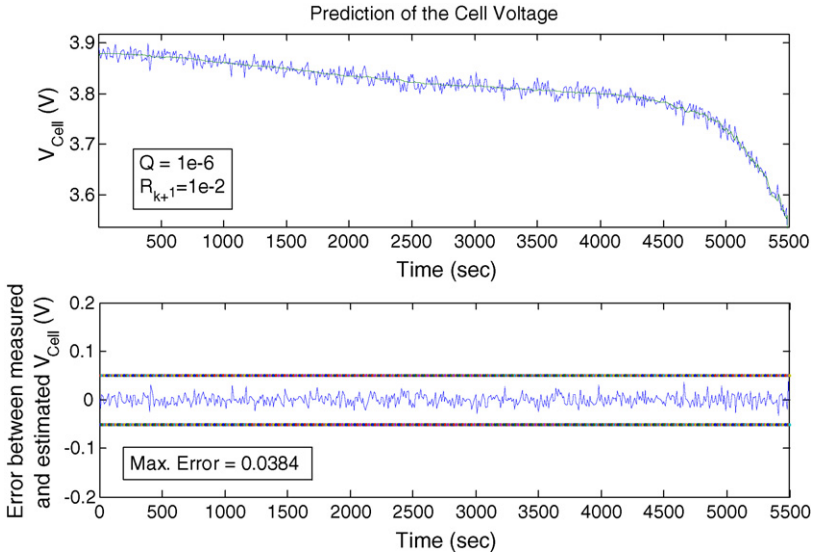

Fig. 2. Cell voltage as a function of time when process noise is negligible.

of the measurement (R_{k+1}) can be used as tuning parameters of the filter. To illustrate this, the model is used to obtain synthetic data for different values of Q and R_{k+1}. The synthetic data was generated by adding zero mean Gaussian noise ($\boldsymbol{G}(t)$), with a standard deviation of 10%, to the discharge curve obtained from the single particle model. Generating data by adding noise to the output of the model is the equivalent of having an error in the cell voltage due to faulty measurements. Hence, a good filter should eliminate the noise due to the measurements and the predicted profile for the cell voltage should not oscillate as much as the noisy data. Two case studies are considered in order to illustrate the capabilities of the present approach. In the first case, all the noise in the data is attributed to the measurement error, consistent with the methodology adopted to generate the synthetic data. In the second case, an incorrect assumption is made that all the noise in the data is from the cell, owing to physical changes happening within the system. Fig. 2 shows the estimated cell voltage as a function of time along with the synthetic data for Case 1. The smooth line through the center is the predicted profile for the cell voltage from the cell. This figure illustrates the capability of the EKF approach to predict the true cell voltage filtering the noise due to the measurements out. There is a good fit between the data and the predictions. The tuning parameters used to generate this data are $Q = 1e{-}6$ and $R_{k+1} = 1e{-}2$. This represents the case where the process noise is insignificant compared to the measurement noise. This is true for the present case, since all the disturbance was added to the true potential (i.e., the actual model predictions) as measurement noise. As a result the estimated voltage does not get perturbed with the experimental noise seen in the data. This verifies the results implied by Eq. (28). Also shown is the error between the two curves as compared to the bounds set by the experimental variance. The error lies well within the bounds of the $3-\sigma$ outliers (shown on either side of the error on the same plot).

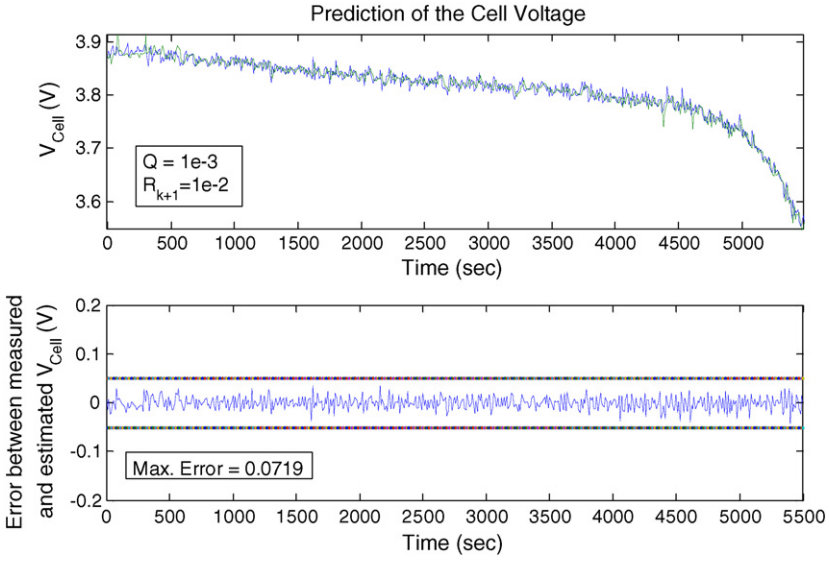

Fig. 3. Cell voltage as a function of time when process noise is considerable.

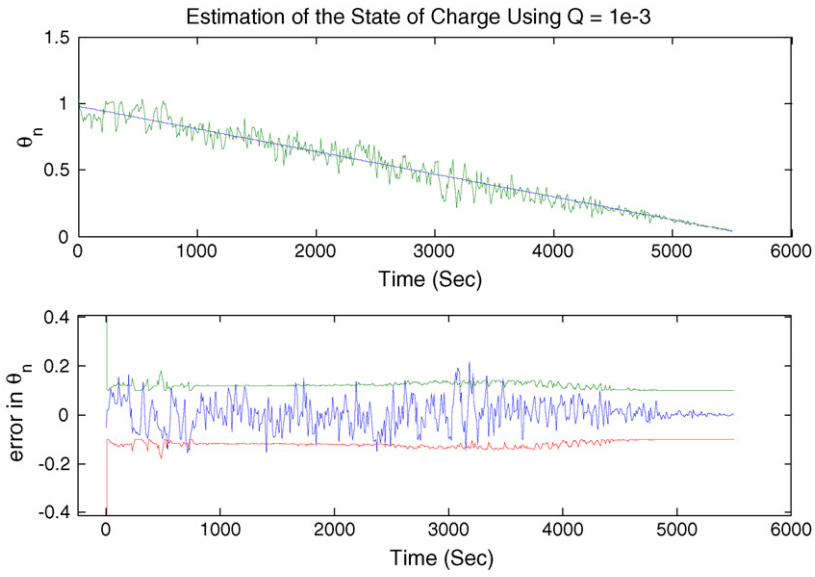

Fig. 4. State of charge as a function of time when process noise is considerable.

Fig. 3 shows the change in V_{cell} with time for Case 2. For this case, we assumed that all the noise is attributed to the process response, i.e., the inadequacy of the model to reflect all the changes that happen within the cell and hence set the penalty on the model (Q) to be 1e−3, which is considerably higher than the previous case. The value of R_{k+1} is the same as in the previous case. These values place less emphasis on the experimental noise and attribute the oscillations in the data to unmodeled dynamics. For this case, one would require that the predicted cell voltage follows the changes in experimental V_{cell} more accurately, since the oscillations in this case are assumed not to originate from measurement error. As seen from Fig. 3 the predicted profile for the cell voltage closely follows the changes in the data as predicted by Eq. (29).

For estimation of the state of charge, Eqs. (33) and (34) were used along with the other model equations to obtain the SOC inside the limiting electrode ($\theta_n(t)$) as shown in Eq. (43). Fig. 4 shows the state of charge calculated using Eq. (43) as a function of time for the second case (i.e., $Q = 1e{-}3$ and $R_{k+1} = 0.01$). This response is noisy and the error is about $\pm 10\%$ as shown by the outliers. The high error in the state of charge estimates reflects our incorrect assumption for Case 2 that the oscillations in the data are due to physical changes into the cell. Note that the synthetic data were generated by adding measurement noise to the true cell potential. Hence, this result is expected. In other words, no process noise was used in generating the synthetic data and all oscillations in the V_{cell} versus t data are because of the measurement noise added to the model. Since the tuning parameters used in Case 2 penalize the model heavily despite its reasonable accuracy, the inaccuracy due to an error in judgment is reflected in the SOC predictions. This inference is further verified in Fig. 5, where the process noise is set to a negligible

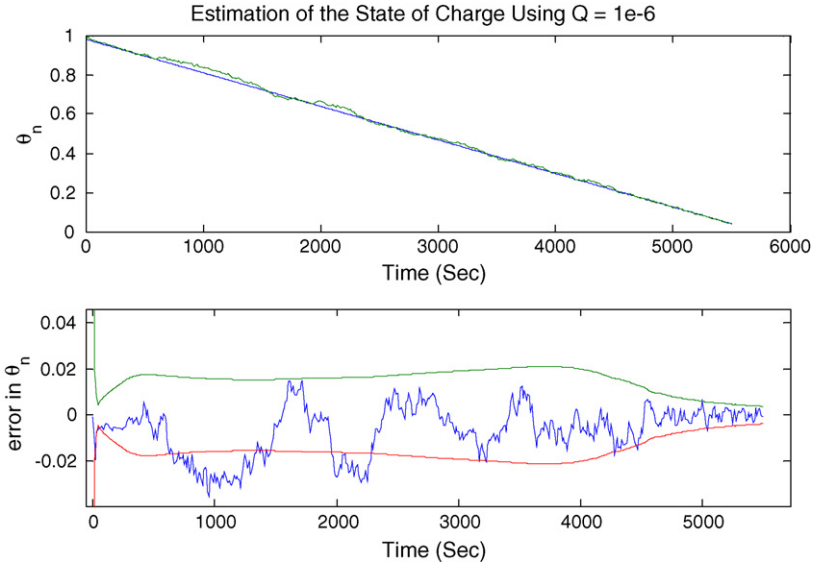

Fig. 5. State of charge as a function of time when process noise is negligible.

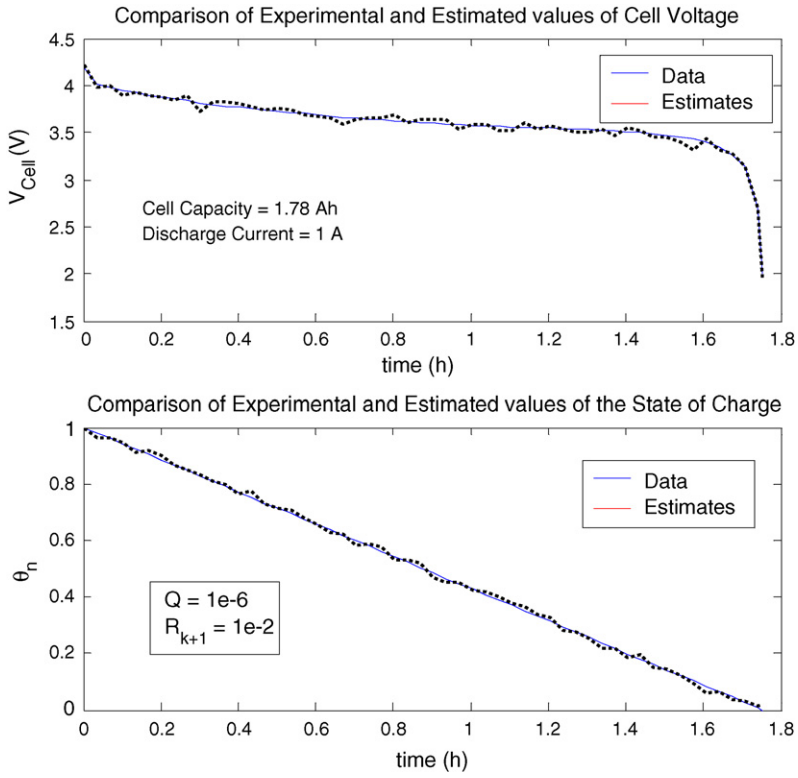

Fig. 6. Comparison of estimates to experimental data.

value (Case 1) and the scatter in the response is attributed to the measurement noise. The state of charge estimate for this case is much smoother and follows closely the values used in the model. The error in the state of charge predictions is about ±2%.

In order to verify the validity of the model, experimental data from Sony 18650 Cells are compared to the estimated cell voltage and state of charge in Fig. 6. The discharge curve was obtained from at 25 °C in an Arbin battery testing system (College Station, TX) at a discharge current of 1 A, after the cell was charged to its full capacity of 1.78 Ah. The data obtained from the experimental discharge curve were used to update the model estimates at each instant of time. The experimental state of charge at each instant of time was obtained by integrating the charge removed from the cell. The values for Q and R_{k+1} were held at 1e−6 and 0.01, respectively. Fig. 6 shows very good agreement between the experimental cell voltage and the predictions.

7. Advantages of the current approach

The methodology outlined in this work does not involve recursive nonlinear regression. The conventional estimation protocols invoke a nonlinear regression technique [39,42], which is a complex iterative process. In order to obtain 'n' parameter values, one needs to solve a minimum of 'n' equations—and since the Kalman filter approach for the estimation of 'n' parameters involves inverting a matrix of size no bigger than 'n', this is the most optimal algorithm to estimate parameters online. Whereas the competitive non-linear least squares algorithm requires about 2.8 s of computational time on a Pentium IV, 2 GHz processor, in order to obtain the state of charge at a particular time, the Kalman filter approach presented here takes about 4 ms for an equivalent estimate. This rapid estimate of the state of charge enables one to follow closely the performance of the cell as shown in Figs. 2–5. Another advantage of the current approach is that it is simple enough to be implemented in a real time device, since it spares the tedium of solving a complex nonlinear optimization problem.

Incorporation of a physics based model along with the Kalman filter based estimation technique improves the predictive capability of the model, in addition to providing a physical insight to the state of charge estimates. For example, the state of charge in the present approach is the ratio between the average concentration to the maximum concentration, of the active material within the electrode that limits the performance of the cell, unlike the empirical values predicted by the models in the literature. Plett [19–21] introduced some models to predict the state of charge of a lithium ion cell accurately using the extended Kalman filter approach. However, results from his work [20] show that it is essential to add an arbitrary number of poles and zeros to the transfer function used to represent the cell in the model, in order to obtain a very good fit. This approach is as empirical as the circuit based approach proposed by others [14–16]. The state of charge predicted by the empirical models does not have a direct correlation with the dynamics of the cell as do the predictions from rigorous models based on the transport and kinetic equations. In addition to this, results from Fig. 6 show that a physics based models can be used to obtain estimates of the state of charge. A Monte Carlo simulation was performed—generating 100 sets of synthetic data and the max-

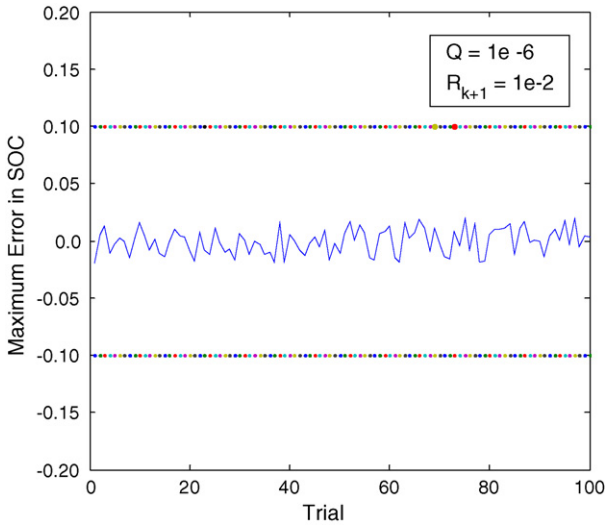

Fig. 7. Maximum error between SOC from model and synthetic data for 100 trials.

imum error in the estimation of the state of charge for each run is plotted in Fig. 7. The results show that for all the cases, the estimates lie well within ±2%.

8. Conclusion

A model-based extended Kalman filter was developed based on a simple electrochemical model of a lithium ion cell. The state of charge of the cell is monitored continuously as a function of time. The predictions were compared with synthetic data. The Kalman filter approach represents the optimal algorithm for recursive identification [16]. The SP model adds the information about the time evolution of the parameters characterizing the system state. Hence, the approach presented here provides estimates of the SOC of the cell, that are as good as any empirical methodology adopted in the literature, while providing a good physical insight into the system. To summarize, the methodology outlined here greatly reduces the computational time involved in obtaining the state of charge from a first principles based model, while adding physical insight into otherwise equivalent circuit based models implementing the filtering technique.

Acknowledgement

The authors gratefully acknowledge the financial support from the National Reconnaissance Office (NRO) under contract #NRO-000-03-C-0122.

References

[1] D. Linden, T.B. Reddy, Handbook of Batteries, third ed., McGraw Hill, NY, 2002.
[2] A. Tenno, R. Tenno, T. Suntio, J. Power Sources 111 (2002) 65–82.
[3] A. Tenno, R. Tenno, T. Suntio, J. Power Sources 103 (2001) 42–53.
[4] E. Meissner, G. Richter, J. Power Sources 116 (2003) 79–98.
[5] F. Huet, J. Power Sources 70 (1999) 56–69.
[6] P. Mauracher, E. Karden, J. Power Sources 67 (1997) 69–94.
[7] H. Blanke, O. Bohlen, S. Buller, R.W. Doncker, B. Fricke, A. Hammouche, D. Linzen, M. Thele, D.U. Sauer, J. Power Sources 144 (2) (2005) 418–425.
[8] A. Hammouche, E. Karden, R.W. Doncker, J. Power Sources 127 (1–2) (2004) 105–111.
[9] J.D. Weiss, US Patent No. 5949219.
[10] V. Mancier, A. Metrot, P. Willmann, J. Power Sources 117 (1–2) (2003) 223–232.
[11] A.T. Stamps, C.E. Holland, R.E. White, E.P. Gatzke, J. Power Sources 150 (2005) 229–239.
[12] T. Hansen, C.-J. Wang, J. Power Source 141 (2005) 351–358.
[13] T. Markel, A. Brooker, T. Hendricks, V. Johnson, K. Kelly, B. Kramer, M. O'Keefe, S. Sprik, K. Wipke, J. Power Sources 110 (2) (2002) 255–266.
[14] M.W. Verbrugge, R.S. Connel, J. Electrochem. Soc. 149 (1) (2002) A45–A53.
[15] M.W. Verbrugge, E. Tate, J. Power Sources 126 (2004) 236–249.
[16] M.W. Verbrugge, B. Koch, J. Electrochem. Soc. 153 (1) (2006) A187–A201.
[17] E.D. Tate, M.W. Verbrugge, B.J. Koch, D.R. Frisch, US Patent Application No. 10/664287.
[18] S. Martinet, R. Durand, P. Ozil, P. Leblanc, P. Blanchard, J. Power Sources 83 (1999) 93–99.
[19] G.L. Plett, J. Power Sources 134 (2004) 252–261.
[20] G.L. Plett, J. Power Sources 134 (2004) 262–276.
[21] G.L. Plett, J. Power Sources 134 (2004) 276–292.
[22] B. Hariprakash, S.K. Martha, A. Jaikumar, A.K. Shukla, J. Power Sources 137 (1) (2004) 128–133.
[23] A.J. Salkind, C. Fennie, P. Singh, T. Atwater, D.E. Reisner, J. Power Sources 80 (1999) 293–300.
[24] K.S. Jeong, W.Y. Lee, C.S. Kim, J. Power Sources 145 (2) (2005) 319–326.
[25] P. Singh, C. Fennie Jr., D. Reisner, J. Power Sources 136 (2) (2004) 322–333.
[26] C. Nanjudaiah, V.R. Koch, Proc. Electrochem. Soc. 90 (5) (1990) 87–97.
[27] Y. Çadirci, Y. Özkazanc, J. Power Sources 129 (2) (2004) 330–342.
[28] S. Piller, M. Perrin, A. Jossen, J. Power Sources 96 (2001) 113–120.
[29] K.E. Thomas, J. Newman, R.M. Darling, in: W.A. van Schalkwijk, B. Scrosati (Eds.), Advances in Lithium-Ion Batteries, Kluwer Academic/Plenum Publishers, NY, 2002, pp. 345–392.
[30] P. Ramadass, B. Haran, M.G. Parthasarathy, R. White, N.P. Branko, J. Electrochem. Soc. 151 (2) (2004) A196–A203.
[31] B.S. Haran, B.N. Popov, R.E. White, J. Power Sources 75 (1) (1998) 56–66.
[32] S. Santhanagopalan, Q. Guo, P. Ramadass, R.E. White, J. Power Sources 156 (2006) 620–628.
[33] G. Ning, N.P. Branko, J. Electrochem. Soc. 151 (10) (2004) A1584–A1591.
[34] Petzold R. Linda, SIAM J. Sci. Stat. Comp. 3 (1982) 367.
[35] J.C. Slattery, Advanced Transport Phenomena, Cambridge University Press, 1999, Chapter 8.
[36] C.Y. Wang, W.B. Gu, B.Y. Liaw, J. Electrochem. Soc. 145 (10) (1998) 3407.
[37] V.R. Subramanian, D. Tapriyal, R.E. White, Electrochem. Sol. State Lett. 7 (9) (2004) A259–A263.
[38] J.O'M. Bockris, A.K.N. Reddy, M.G. Aldeco, Modern Electrochemistry, 2A, second ed., Kluwer Academic/Plenum Publishers, NY, 2000.
[39] Y. Bard, Nonlinear Parameter Estimation, Academic Press, NY, 1974.
[40] Q. Guo, R.E. White, J. Electrochem. Soc. 152 (2) (2005) A343–A350.
[41] J.D. Francis III, M.A. Henson, in: M.A. Henson, D.E. Seborg (Eds.), Nonlinear Process Control, Prentice Hall PTR, NJ, 1997, Chapter 3.

[42] A. Constantinidis, N. Mostoufi, Numerical Methods for Chemical Engineers with MATLAB Applications, Prentice-Hall, Upper Saddle River, NJ, 1999.
[43] D.R. Smith, SIAM Rev. 29 (1) (1987) 91–113.
[44] P. Arora, M. Doyle, R.E. White, J. Electrochem. Soc. 146 (10) (1999) 3543–3553.
[45] J.L. Crassidis, J.L. Junkins, Optimal Estimation of Dynamic Systems, Chapman & Hall/CRC Applied Mathematics and Nonlinear Science Series, NY, 2004.
[46] Determining Covariances from Data, J.B. Rawlings, Exxon Mobil Workshop on State Estimation and Nonlinear Control, TX, 2004, see: http://jbrwww.che.wisc.edu.